

DDS: Decoupled Dynamic Scene-Graph Generation Network

A S M Iftekhar*, Raphael Ruschel*, Satish Kumar, Suya You, B. S. Manjunath

Abstract—Scene-graph generation involves creating a structural representation of the relationships between objects in a scene by predicting subject-object-relation triplets from input data. However, existing methods show poor performance in detecting triplets outside of a predefined set, primarily due to their reliance on dependent feature learning. To address this issue we propose DDS— a decoupled dynamic scene-graph generation network— that consists of two independent branches that can disentangle extracted features. The key innovation of the current paper is the decoupling of the features representing the relationships from those of the objects, which enables the detection of novel object-relationship combinations. The DDS model is evaluated on three datasets and outperforms previous methods by a significant margin, especially in detecting previously unseen triplets.

Index Terms—Activity detection, compositional learning, zero-shot learning, scene graphs, scene understanding.

I. INTRODUCTION

DYNAMIC Scene-Graph (DSG) provides a graph structure presenting the relationships among different objects in a scene. It aims to create the scene-graph by predicting relationship triplets composed of $\langle \text{subject}, \text{object}, \text{relationship} \rangle$ at each frame of an input video. This acts as a foundational block for various computer vision tasks [1], [2]. Current DSG generation systems [3]–[5] operate in a constrained setting where the possible triplets are predefined for a given set of relationships and objects. However, in a more realistic deployment scenario, it is likely that the network will encounter triplets that it has not seen before. Therefore, a system should be able to transfer the learned concepts of relationships and objects to compose unseen triplets. Our analysis has shown (Table I) poor performance in detecting these unseen triplets using the state-of-the-art (SOTA) method. This poor performance is mainly attributed to the learning of highly dependent feature representations of relationships and objects. The proposed decoupled dynamic scene-graph (DDS) addresses this issue.

Fig. 1 shows the core idea of the proposed DDS network. This architecture utilizes two different branches to learn decoupled features for relationships and objects. As shown in the

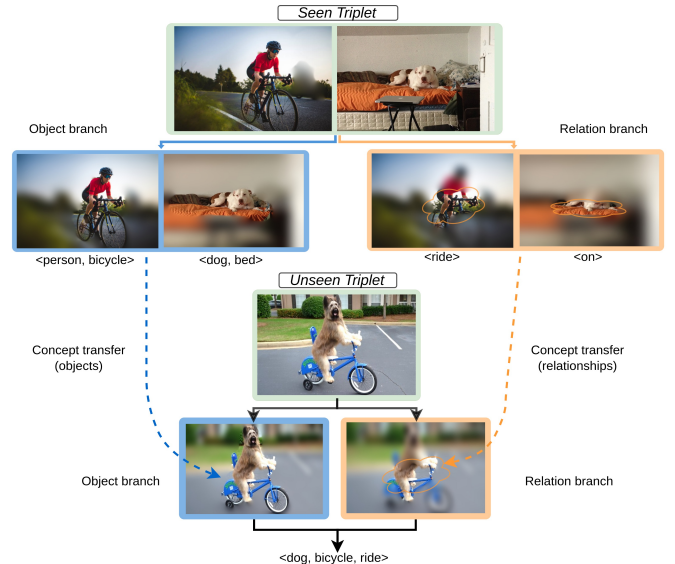


Fig. 1. Diagram to show the concept learning and transferring in DDS. By focusing on different spatial regions, DDS learns the concept of relationships (ride, on) and objects (person, bicycle, bed) independently. In the lower section of the diagram, we show how these learned concepts are transferred and utilized to detect the unseen triplet $\langle \text{dog}, \text{bicycle}, \text{ride} \rangle$.

figure, DDS learns the concept of ‘ride’, ‘on’, ‘person’, ‘bicycle’, and ‘bed’ from the training examples of a ‘person riding a bike’ and a ‘dog on the bed’ independently. The decoupled design makes DDS look into different spatial regions for relationships and objects. These learned concepts are transferred to successfully detect the unseen triplet $\langle \text{dog}, \text{bicycle}, \text{ride} \rangle$, see Section V-C for more details.

Existing works [3]–[5] for generating DSGs follow a two-stage process. First, an object detector localizes objects irrespective of their relationship status. In the second stage, different attention-based [3], [4] and graph-based [5] methods utilize features extracted from the previously localized objects to predict relationships. In this process, the extracted features of the objects are fed throughout the network for relationship detection. As a result, these methods learn to associate a relationship only with a particular combination of objects and hence perform poorly to predict unseen triplets.

In contrast, DDS ensures the learning of discriminative spatio-temporal cues for relationships and objects. Fig. 2 shows the overview of our architecture. It consists of two separate branches: the relation and the object branch. We chose a Transformer based encoder-decoder [6] architecture for these branches with two different sets of queries. Moreover, a novel

* represents equal contribution.

A S M Iftekhar, Raphael Ruschel, Satish Kumar, and B.S. Manjunath are with the Department of Electrical and Computer Engineering, University of California Santa Barbara, Santa Barbara, CA, 93106. E-mail: {iftkhar, raphael251, satishkumar, manj}@ucsb.edu

Suya You is with Army Research Laboratory, Intelligent Perception, CISD Los Angeles, CA. Email: suya.you.civ@army.mil

temporal decoder is added to embed temporal information into the queries. These separate sets of queries focus on learning generalized representations for relationships and objects from differently encoded feature maps in both temporal and spatial domains. This is significantly better than the existing works, where the same object features are used for both object and relationship detection. Also, DDS does not have the dependence on the off-the-shelf object detectors like previous works.

Our proposed model is thoroughly evaluated on the Action-Genome [7] dataset for DSG generation, where it achieves significant performance gains compared to the SOTA models. Additionally, we evaluate DDS on the task of static scene-graph (SSG) generation on the HICO-DET [8] dataset and unusual SSG generation on the UnRel [9] dataset, where DDS outperforms all the existing models in both datasets. Finally, the proposed design choices are evaluated in an extensive ablation study.

II. RELATED WORKS

DDS is built on the previously developed works in SSG and DSG generation. This section is used to review the literature in the mentioned areas along with additional relevant publications on scene-graph generation under the compositional setting.

A. Static Scene-Graph (SSG) Generation

SSG generation is proposed by [10] for the task of image retrieval. An extensive literature exists [11]–[32] in this area. The initial works [21]–[26] rely heavily on two-stage (object detection and then scene-graph generation) structures. Few of these works utilize different recurrent neural network (RNN) variants [33], [34] while other prominent researches focus on graph structure [20], [25], [26] with attention mechanisms. Also, many authors utilize prior knowledge [26], [29], [35] (e.g. semantic knowledge, statistical heuristics) for SSG generation. Despite recent improvements in SSG generation, these methods are heavily constrained by their reliance on the object detection quality as noted in [36].

Modern works [36]–[46] in SSG generation focus on utilizing a one-stage Transformer based architecture to deal with the aforementioned issues. These approaches mainly focus on human-object interaction (HOI) detection. HOI detection is a subtask of SSG generation where the relationships among objects are limited to interaction verb [3], such as hold, work, talk. These methods employ one-stage Transformer based encoder-decoder architectures following the architecture from DETR [6]. These architectures rely on set-based predictions to generate SSG. Among these works, Qpic [38] uses a single encoder-decoder model while CDN [42] extends Qpic by using sequential decoding of objects and relationships. Additionally, MSTR [41] enables the use of multi-scale feature maps to these networks. Another concurrent work, SSRT [36] refines the overall architecture with spatial and semantic support features. Moreover, a recent line of research heavily exploits the usage of very large-scale semantic knowledge engines (e.g. CLIP [47]) [36], [43], [46]. Also, few works propose to utilize different types of post-processing steps [46] for

the task. Apart from the obvious limitation of these works being unable to utilize temporal dependencies, they perform poorly while detecting unseen triplets. With the decoupled multi-branch design, we significantly differ from these works by using separate sets of queries for relationship and object detection.

B. Dynamic Scene-Graph (DSG) Generation

DSG is an extension of the SSG where the scene-graph is created for videos. This process is harder since temporal cues need to be utilized [3]–[5]. Current works in this area have two-stage architectures following the initial works on SSG. Among these works, STTran [5] utilizes a temporal decoder based on the self-attention mechanism. DSGAP [4] expands STTran with an anticipatory pre-training paradigm. On the other hand, HORT [3] utilizes a multi-branch design with different types of Transformers.

Both STTran and HORT use similar features for relationship and object detection. These features come from the object bounding boxes predicted by off-the-shelf object detectors. STTran concatenates pair-wise object features to use as relationship features whereas HORT pools relationship features from a joint box of object pairs. However, using similar features for relationship and object detection forces the learning of relationships and objects to be dependent on each other. Therefore, to ensure generalized learning, we focus on learning the features independently.

C. Compositionality in Scene-Graph Generation

Creating new compositions from base known concepts during inference is known as compositional zero-shot learning (CZSL) under the compositional setting [48]–[52]. In this paper, we utilize this setting to evaluate our model. Kato et al. [53] introduce CZSL in SSG generation with an embedding-based model. Many following works [54]–[56] adapt different object-affordance ideas. These works assume there exist common relationships between the subjects and the objects. This work does not have such limited assumptions, and as a result, is able to generate scene graphs even when the relationships are very unusual (See Table IV).

III. METHOD

This section describes the developed model for the problem of dependent feature learning in DSG generation that makes current models perform poorly in detecting unseen relationship triplets. This work proposes a multi-branch network that learns distinct feature representations for relationships and objects to improve upon this limitation. Before going into the details of the architecture, the problem will be formulated in detail first.

A. Problem Formulation

Given an input video, $\mathbf{V} = \{\mathbf{I}_1, \mathbf{I}_2, \dots, \mathbf{I}_t, \dots, \mathbf{I}_T\}$ with T frames, the task in DSG generation is to predict a set of relationship triplets, $\{R_1, R_2, \dots, R_t, \dots, R_M\}$ at every frame of the video. Every frame has N_M number of relationship triplets. Each relationship triplet can be presented by $\langle s, o, r_{so} \rangle$. Here,

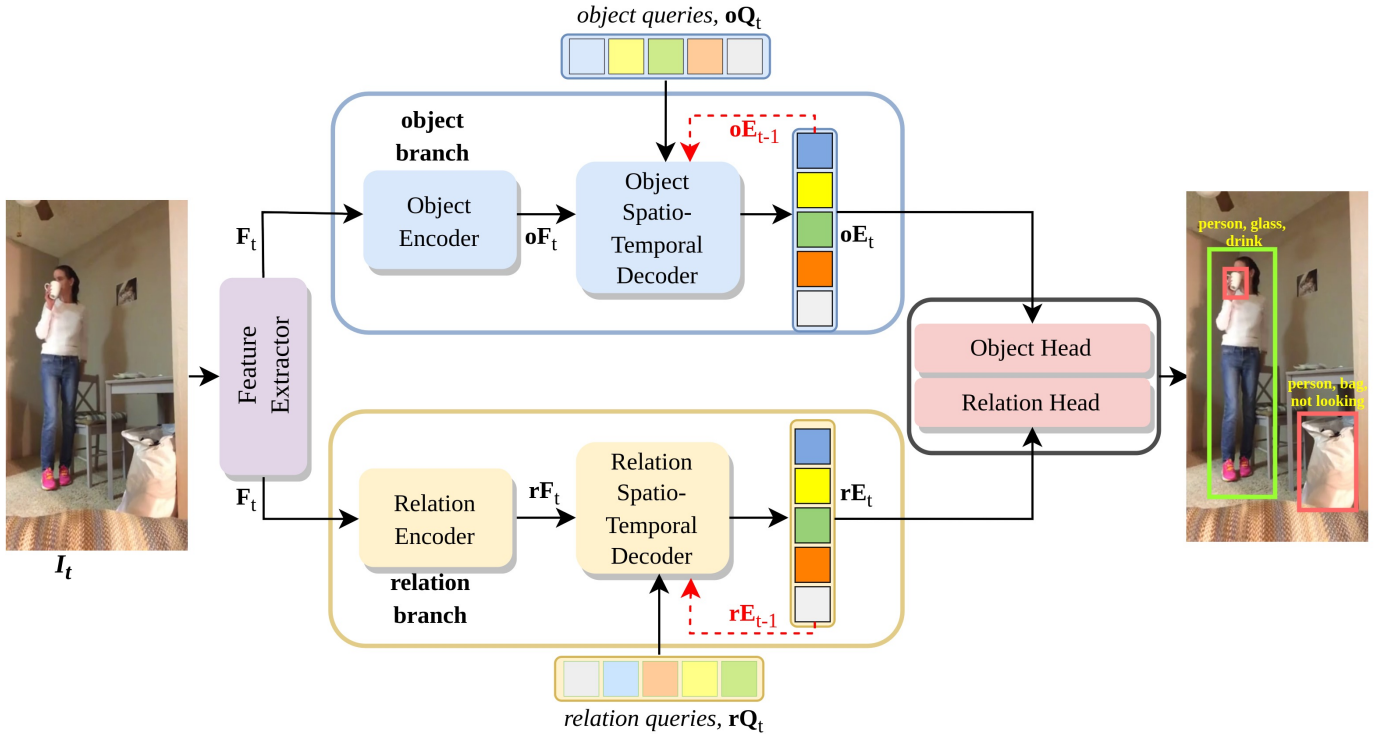


Fig. 2. Overview of DDS’s architecture. Given an input frame I_t , features are extracted by the backbone. These features are fed to the object and the relation branch. These decoupled branches consist of an encoder and a spatio-temporal decoder. Encoders from both branches encode the feature maps differently and send them to the decoders. Each spatio-temporal decoder takes a set of queries (object/relation) along with the previous frame’s embeddings (shown by the red arrow). The output of the spatio-temporal decoders are learned embeddings. These learned embeddings are fed to the object and the relation heads to predict relationship triplets.

s , o refers to subject, object and are represented by bounding boxes and category labels. r_{so} is the relationship between s and o . In a single frame I_t , s and o can have multiple relations, as shown in the sample input-output pair in Figure 2.

In this paper, the main goal is to predict relationship triplets under the compositional setting. In this setting the test set contains triplets that are not present in the training set. Consider having in total N_o number of objects and N_r number of relations. The training set has N_s number of relationship triplets composed from the mentioned N_o objects and N_r relationships. On the other hand, the test set has N_u number of unseen triplets not present in the training set in addition to the N_s number of seen triplets, where all the unseen triplets are composed of the same N_o objects and N_r relationships.

B. Technical Overview

The proposed work adopts a one-stage approach for DSG generation compared to the current two-stage methods [3]–[5] as the former [37]–[40] have shown impressive performance in creating SSG. However, these image-based works present poor generalization capabilities. Therefore, we propose a network that uses a different set of queries with two branches: the relation branch and the object branch. Each branch follows a Transformer-like encoder-decoder architecture. Fig. 2 shows a diagram of the model, where a convolutional neural network (CNN) extracts features from the input frame, and those are encoded differently by the object and the relation encoders. Each spatio-temporal decoder takes encoded features from

their respective encoder in addition to two types of inputs: queries for the current frame (oQ_t , rQ_t) and the embeddings (oE_{t-1} , rE_{t-1}) propagated from the previous frame. As the encoded features differ for each branch, the queries learn decoupled features for relationships and objects. The decoder outputs are the learned object and relation spatio-temporal embeddings. These embeddings are sent to the relation and the object heads for final predictions. Moreover, these embeddings are propagated to the next frame of the video.

C. Feature Extraction & Encoders

Consider a frame $I_t \in \mathbb{R}^{N_C \times H \times W}$ at time t of the input video V . Here, N_C , H , W are the number of channels, height, and width of the frame, I_t . DDS uses a CNN network as backbone, \mathbf{B} (e.g. resnet-50 [57]) to extract features $\mathbf{B}(I_t) \in \mathbb{R}^{N_{C'} \times H' \times W'}$ from the input frame. Then, 1×1 convolution is used to reduce the channel dimension from $N_{C'}$ to d . After that, a flattening operation is performed and a fixed positional embedding is added to $\mathbf{B}(I_t)$ like existing works [37]–[40] to get the feature map $\mathbf{F}_t \in \mathbb{R}^{(H'W') \times d}$. These embeddings express each spatial position of the feature map in high dimensions [6]. DDS uses \mathbf{F}_t as a common feature for both the relation and the object branches.

Both of the network’s branches have an encoder comprising of stacked multi-head self-attention layers [58] with a feed-forward network (FFN). The output of the encoders are two

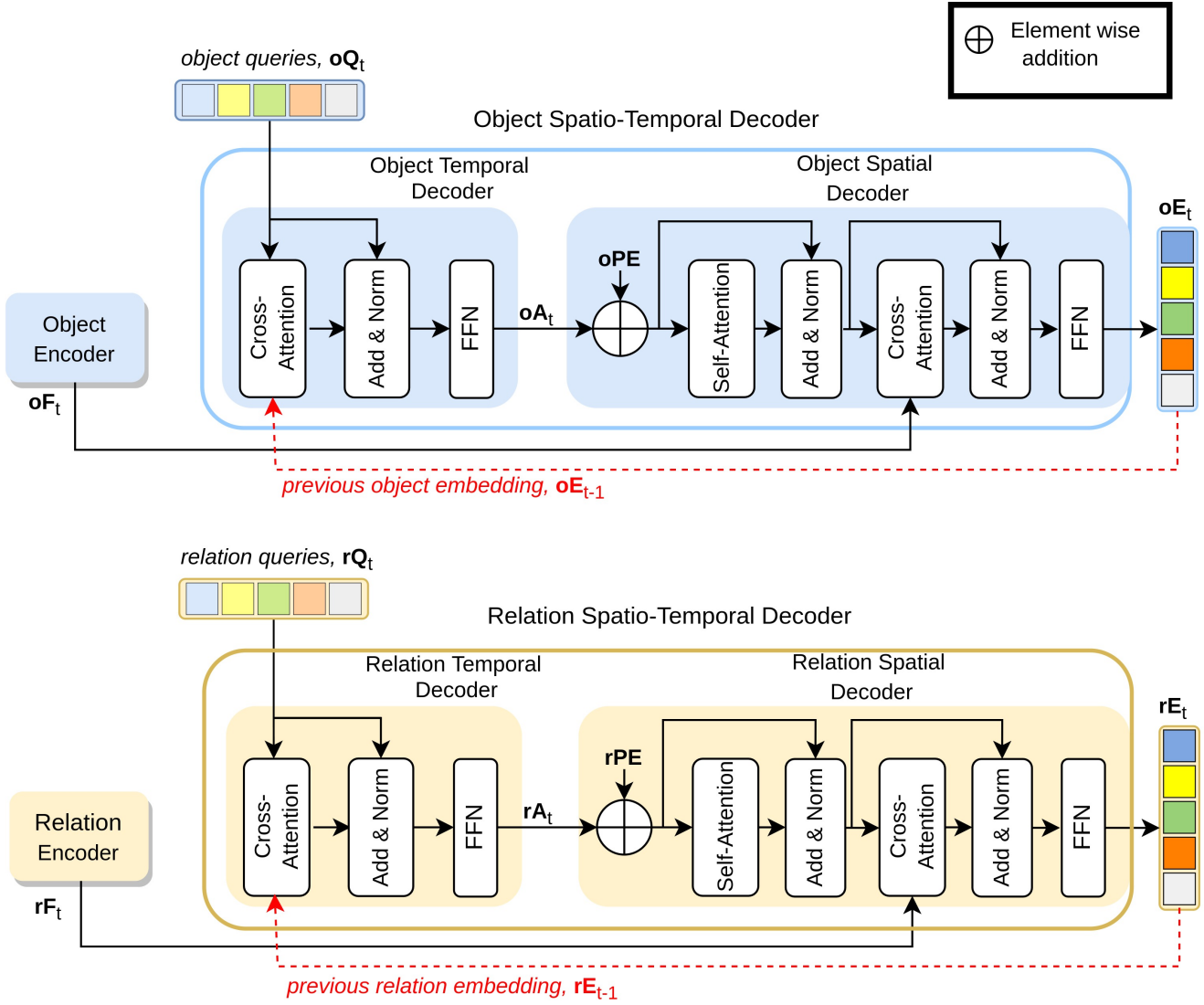


Fig. 3. Design of the spatio-temporal decoders. Every spatio-temporal decoder is composed of a temporal and a spatial decoder. Each decoder converts a different set of queries into learned embeddings while making sure decoupled learning in each branch.

separate feature maps,

$$\mathbf{rF}_t = \text{Relation Encoder}(\mathbf{F}_t) \quad (1)$$

$$\mathbf{oF}_t = \text{Object Encoder}(\mathbf{F}_t) \quad (2)$$

Here, \mathbf{rF}_t , \mathbf{oF}_t refer differently encoded versions of the feature map \mathbf{F}_t . Our spatio-temporal decoders will utilize these feature maps for decoupled learning.

D. Spatio-Temporal Decoders

DDS's spatio-temporal decoders convert a set of learnable queries into output embeddings. This transformation occurs in two stages. In the first stage, the current frame's queries attend to the previous frame's output embeddings to aggregate temporal information. In the second stage, these aggregated queries gather information from the encoded feature maps of the current frame. The proposed multi-branch design ensures discriminative feature learning for the queries of each branch. Each decoder consists of two small components: temporal and spatial decoder. Please see Fig. 3 for reference.

Temporal Decoders: These decoders allow queries to leverage temporal dependencies. Each temporal decoder takes two sets as inputs: the current frame's queries and the embeddings from the previous frames. For frame \mathbf{I}_t , the current frame's relation and object queries sets are defined as $\mathbf{rQ}_t \in \mathbb{R}^{N_q \times d}$ and $\mathbf{oQ}_t \in \mathbb{R}^{N_q \times d}$. Every query is a d dimensional vector, and every branch has N_q number of queries. Embeddings from the previous frames for the relation and the object branches are presented by $\mathbf{rE}_{t-1} \in \mathbb{R}^{N_q \times d}$ and $\mathbf{oE}_{t-1} \in \mathbb{R}^{N_q \times d}$, and are marked with a red arrow in Fig.3.

Temporal decoders are made of stacked multi-head cross-attention layers [6] with an FFN network. The cross-attention in the temporal decoders allows the current frame's queries to select what to learn from the previous frame's embeddings. The outputs of the temporal decoders are the temporally aggregated queries \mathbf{rA}_t , \mathbf{oA}_t . They are fed to their respective spatial decoders. In the case of the first frame of a video, the temporal decoders directly output \mathbf{rQ}_t and \mathbf{oQ}_t as \mathbf{rA}_t and \mathbf{oA}_t without passing them through the cross-attention and

FFN blocks as there is no previous frame in this case.

Spatial Decoders: The spatial decoders architecture is similar to the standard Transformer decoder [6]. These decoders consist of both self-attention and cross-attention layers along with FFN networks. Each decoder takes encoded feature maps (\mathbf{rF}_t or \mathbf{oF}_t) along with the aggregated queries of the temporal decoders (\mathbf{rA}_t or \mathbf{oA}_t) from their respective branch as inputs. Also, these decoders take learnable positional embeddings. These embeddings for the relation and the object branch are defined as $\mathbf{rPE} \in \mathbb{R}^{N_q \times d}$, $\mathbf{oPE} \in \mathbb{R}^{N_q \times d}$.

$$\mathbf{rE}_t = \text{Relation Decoder}(\mathbf{rN}_t, \mathbf{rPE}, \mathbf{rQ}_t) \quad (3)$$

$$\mathbf{oE}_t = \text{Object Decoder}(\mathbf{oN}_t, \mathbf{oPE}, \mathbf{oQ}_t) \quad (4)$$

The outputs of the decoders are the learned spatio-temporal embeddings. They are used in the object and the relation heads to make the final relationship triplet predictions. Also, each spatial decoder's output is fed to the next frame's temporal decoder as previous embeddings.

Both spatial and temporal decoders keep the separation in feature learning for relationships and objects using different encoded features, set of queries, and previous embeddings. As a result, the output embeddings from the decoders are decoupled generalized representations.

E. Object Heads

The output embeddings from the object spatio-temporal decoder, \mathbf{oE}_t are fed to four different FFNs. For input frame \mathbf{I}_t , these FFNs predict subject bounding boxes, $\mathbf{sB}_t \in [0, 1]^{N_q \times 4}$, object bounding boxes, $\mathbf{oB}_t \in [0, 1]^{N_q \times 4}$, subject prediction vectors, $\mathbf{sP}_t \in [0, 1]^{N_q \times O}$, and object prediction vectors, $\mathbf{oP}_t \in [0, 1]^{N_q \times N_o}$. Here, N_q is the number of queries, and N_o is the total number of objects.

F. Relation Heads

Like the object heads, the learned output embeddings, \mathbf{rE}_t , are fed to two FFNs that produce as output the relation prediction vectors, $\mathbf{rP}_t \in [0, 1]^{N_q \times N_r}$ and relation region bounding boxes $\mathbf{rB}_t \in [0, 1]^{N_q \times 4}$. Here, N_q is the number of queries, and N_r is the total number of relationships under consideration. Notice that the relation region bounding box is defined as the union between the subject and object bounding boxes.

G. Inference

We compose N_q relationship pairs by one-to-one matching of \mathbf{sB}_t and \mathbf{oB}_t . One-to-one matching refers to matching the q -th prediction from \mathbf{sB}_t with the q -th prediction from \mathbf{oB}_t . Moreover, for every prediction vector in \mathbf{sP}_t and \mathbf{oP}_t , the maximum confidence score is used to create $\mathbf{sP}_{tmax} \in [0, 1]^{N_q}$ and $\mathbf{oP}_{tmax} \in [0, 1]^{N_q}$ and the corresponding index is used to determine the category label for each of the bounding boxes. For every composed relationship pair, the final relation score prediction vectors are calculated as:

$$\mathbf{rP}_{tfinal} = \mathbf{rP}_t * \mathbf{sP}_{tmax} * \mathbf{oP}_{tmax} \quad (5)$$

H. Training

For training DDS, we utilize losses similar to Qpic [38]. This loss calculation implicitly binds the two sets of queries from the relation and the object branch. The loss calculation happens in two stages:

In the first stage, we find the bipartite matching between the predictions and the ground truths. First, the total prediction set for the input frame \mathbf{I}_t as, $\mathbf{P}_t = \{\mathbf{sB}_t, \mathbf{oB}_t, \mathbf{sP}_t, \mathbf{oP}_t, \mathbf{rB}_t, \mathbf{rP}_t\}$ is generated. This yields N_q number (equal to the number of queries in each branch) of predictions. N_q is chosen in such a way that it is always greater than the number of ground truths per frame. We pad ground truths with ϕ (no relationship triplet) so that it is possible to have the ground truth set \mathbf{G}_t with N_q number of elements. One important detail to note here is that there are three kinds of ground truth bounding boxes: subject bounding boxes, object bounding boxes, and relation regions. Ground truth relation regions refer to the union bounding boxes between the subject and the object bounding boxes that have relations, and are only used during the training phase. Next, each element in \mathbf{P}_t is matched with an element from the ground truth set, \mathbf{G}_t . The matching cost metrics is, $\mathbf{C} \in \mathbb{R}^{[N_q \times N_q]}$. Any element (i, j) in this metrics refers to the cost to match i^{th} element from \mathbf{P}_t with j^{th} element from \mathbf{G}_t and defined as,

$$\mathbf{C}^{(i,j)} = \eta_b(\mathbf{C}_{sb}^{(i,j)} + \mathbf{C}_{ob}^{(i,j)} + \mathbf{C}_{rb}^{(i,j)}) + \eta_o \mathbf{C}_o^{(i,j)} + \eta_r \mathbf{C}_r^{(i,j)} \quad (6)$$

$\mathbf{C}_{sb}^{(i,j)}$, $\mathbf{C}_{ob}^{(i,j)}$, $\mathbf{C}_{rb}^{(i,j)}$ are the subject bounding box, the object bounding box and the relation region matching costs, $\mathbf{C}_o^{(i,j)}$ is the object label matching cost, and $\mathbf{C}_r^{(i,j)}$ is the relation label matching cost between i^{th} element from \mathbf{P}_t and j^{th} element from \mathbf{G}_t . These costs are calculated following [38]. η_b, η_o, η_r are fixed hyper-parameters. The Hungarian matching algorithm [6] is used to find the optimal matching between the predictions and the ground truths by using these cost metrics. After this matching, every prediction is associated with a ground truth. Next, the following loss is calculated for training the network:

$$\mathcal{L} = \lambda_g \mathcal{L}_{GIOU} + \lambda_l \mathcal{L}_{L1} + \lambda_o \mathcal{L}_{obj} + \lambda_r \mathcal{L}_{rel}, \quad (7)$$

Here, \mathcal{L}_{GIOU} and \mathcal{L}_{L1} are the generalized intersection over union (gIOU) and L1 box regression losses for the predicted subject bounding boxes, object bounding boxes, and relation regions. \mathcal{L}_{obj} is the cross-entropy loss for subject and object label predictions. \mathcal{L}_{rel} is the binary cross-entropy loss for the relationship label predictions. $\lambda_o, \lambda_g, \lambda_l$, and λ_r are the corresponding hyper-parameters.

Notice that a portion of the datasets [7], [8] fixes the subject as humans. In this case, the subject prediction vectors and subject bounding boxes are not used for loss calculation.

IV. EXPERIMENTS

A. Experimental Setup

We evaluate DDS's performance in Action Genome (AG) [7] dataset. Moreover, we show our model's performance in SSG generation datasets: HICO-DET [8] and UnRel [9]. As these datasets only contain images, each sample is treated as a

	Seen		Unseen	
	R@20	R@50	R@20	R@50
STTran [5]*	33.7	36.6	0.3	4.4
DDS (Ours)	41.8	48.8	7.4	18.2

TABLE I

DDS’S PERFORMANCE COMPARISON IN AG TEST SET UNDER THE COMPOSITIONAL SETTING. BOTH REPORTED MODELS ARE TRAINED ON THE PROPOSED SMALL-SIZE TRAINING SET UNDER THE COMPOSITIONAL SETTING. * MEANS THE MODEL WAS TRAINED USING PUBLICLY AVAILABLE CODE. AMONG RECENT DSG GENERATION MODELS, ONLY STTRAN’S [5] CODE IS PUBLICLY AVAILABLE. THE BEST RESULTS ARE SHOWN IN **BOLD**.

Method	Backbone	R@20	R@50
GPNN [59]	ResNet-101	33.3	42.6
PPDM [60]	Hourglass-104	34.1	43.5
VRD [61]	ResNet-101	22.0	32.7
IMP [33]	ResNet-101	34.4	43.7
MSDN [62]	ResNet-101	34.7	43.8
Graph RCNN [63]	ResNet-101	35.0	44.1
RelDN [12], [64]	ResNet-101	35.1	44.9
VCTree [12]	ResNet-101	35.0	44.3
STTran [5]	ResNet-101	36.2	48.8
HORT [3]	ResNet-101	36.5	46.7
DSGAP [4]	ResNet-101	37.9	50.1
DDS (Ours)	ResNet-50	43.3	51.5

TABLE II

DDS’S PERFORMANCE COMPARISON IN AG TEST SET. HERE, LIKE OTHER MODELS, DDS IS TRAINED IN THE FULL TRAINING SET OF AG DATASET. THE BEST RESULTS ARE SHOWN IN **BOLD**. FOR THE OTHER MODELS, ALL THE REPORTED NUMBERS ARE TAKEN FROM THE ORIGINAL PUBLICATIONS.

single-frame video. Next, the used datasets will be presented in more detail:

Action Genome (AG) [7]: This dataset is built on top of the Charades [67] dataset, provides frame-level annotations, and is extensively used in the literature for DSG generation. It has 36 distinct object classes and 25 relationship classes. The object classes are common household items such as doors, windows, and cups, and have a total (train and test set) of 476, 229 bounding boxes. The relationship classes are divided into 3 distinct sub-types: (1) *Attention* relationship denotes if the subject is looking at an object. (2) *Spatial* relationship denotes the spatial location of the object with respect to the subject, for example, above, or below. (3) *Contacting* relationship represents how the object is being contacted by the subject. In total, AG provides 1, 715, 568 instances of the mentioned classes contained in 135, 484 subject-object pairs. Every subject-object pair can have multiple relations. Also, on AG the subject class is always human.

Originally, the AG dataset provided 7, 464 videos with 166, 785 frames in the training set and 1, 737 videos with 54, 371 frames in the test set. The original training set contains 530 relationship triplets. All these relationship triplets are present in the test set. We refer to this setting as the fully-supervised setting. As the main interest in this paper is to evaluate DDS’s performance in the compositional setting, a new training split of the data is created. This new proposed training set contains 6, 784 videos with 146, 517 frames con-

Method	Unseen (mAP)	Seen (mAP)	Full (mAP)
VCL [30]	10.1	24.3	21.4
ATL [54]	9.2	24.7	21.6
FCL [56]	13.2	24.2	22.0
THID [65]	15.5	24.3	23.0
SCL [55]	19.1	30.4	28.1
DDS (Ours)	21.1	31.7	29.6

TABLE III

DDS’S PERFORMANCE COMPARISON IN HICO-DET TEST SET UNDER RF (RARE-FIRST) COMPOSITIONAL SETTING. THE BEST RESULTS ARE SHOWN IN **BOLD**.

Method	Unseen (mAP)	Seen (mAP)	Full (mAP)
VRD [61]	-	-	7.2
WSL [9]	-	-	9.9
DUV [66]	-	-	13.4
DDS (Ours)	16.3	27.4	17.9

TABLE IV

DDS’S PERFORMANCE COMPARISON IN UNREL TEST SET. THE BEST RESULTS ARE SHOWN IN **BOLD**. NOT REPORTED RESULTS ARE MARKED WITH -.

taining 421 relationship triplets. The original test set is not changed. It contains 499 object-relationship, where 80 of them are not present in our new training set.

HICO-Det [8]: This dataset has 80 objects and 117 relationship classes. The relationships are limited to interactions such as holding, working, etc. In the literature, this dataset is used for evaluating SSG generation performance under compositional setting [30], [54]–[56]. DDS’s performance is reported following the RF (Rare First) protocol provided by [30]. This protocol has 37, 328 images in the training set with 480 relationship triplets. The test set has 9, 552 images with 480 seen relationship triplets and 120 unseen relationship triplets.

UnRel [9]: This dataset provides extremely unusual SSG triplets, for example: $((elephant, bike, riding))$. It has 4000 training and 1000 test images with 100 objects and 70 relationships. The original train/test split provided by the authors already provides a compositional setting where the test set has 65 unseen relationship triplets. The training set contains 4000 seen relationship triplets.

B. Evaluation Metrics

Following existing works [3]–[5], [7], we report our performances in AG dataset with Recall@K metric. Here, $K = [20, 50]$. We utilize the most challenging SGGDet [7] protocol to report our performances. In this protocol, the network needs to detect relationship triplets along with subject and object bounding boxes. There can be multiple relationship triplets between a subject-object pair. Moreover, mAP (mean average precision) was selected to report the performances in UnRel and HICO-Det datasets similar to current works [9], [54], [56], [66]. Here, performances are reported in three categories: unseen (only unseen relationship triplets), seen (only seen relationship triplets), and full (all relationship triplets) [30]. For all datasets, a prediction triplet from DDS is considered correct if subject and object bounding boxes have at least 0.5 Intersection over Union (IoU) with ground truth bounding

Type	Relation Region	Separate Encoders	Separate Spatio-temporal Decoders	Unseen (mAP)	Seen (mAP)
Single branch (base network)	✗	✗	✗	17.9	29.9
	✗	✗	✓	18.7	30.5
Multi branch	✗	✓	✓	19.7	31.6
	✓	✓	✓	21.1	31.7

TABLE V
IMPACT OF DIFFERENT COMPONENTS ON OUR DECOUPLED MULTI-BRANCH DESIGN.

	Unseen (mAP)	Seen (mAP)
DDS with o to r	19.6	30.6
DDS with r to o	19.4	28.8
DDS with separate queries	21.1	31.7

TABLE VI
DIFFERENT KINDS OF QUERY SHARING STRATEGY. O TO R REFERS TO OBJECT TO RELATION BRANCH QUERY SHARING. R TO O REFERS TO RELATION TO OBJECT BRANCH QUERY SHARING.

Relation Region	Sub-Obj IoU, θ	Unseen (mAP)	Seen (mAP)
	0	19.2	30.3
Mixture	0.1	18.0	30.4
	0.5	19.4	30.8
Union Box	-	21.1	31.7

TABLE VII
DIFFERENT KINDS OF RELATION REGION GROUND TRUTHS. SUB-OBJ IOU REFERS TO THE IOU BETWEEN THE SUBJECT AND THE OBJECT BOUNDING BOXES.

boxes and subject, object, and relationship labels match with ground truth labels.

C. Implementation details

ResNet-50 [57] is used as the CNN backbone. Both temporal decoders inside the spatio-temporal decoders have a single layer. We follow Qpic’s [38] setup for the encoders. We select 6 layers for the object spatial decoder with 3 layers for the relation spatial decoder. All loss coefficients in equation 6 and equation 7 are set as [38]. The number of queries in each branch is 64. Each query is a vector of size 256. The model is trained with AdamW [68] optimizer. We initialize the parameters of DDS from DETR [6] trained on COCO [69] object detection dataset. The initial learning rate for the backbone network is 10^{-6} and for the other part of the network is 10^{-5} .

When training in the AG dataset, we drop the learning rate by 10 times at every 40 epochs and utilize a batch size of 128. DDS processes each video frame from a single video sequentially. We utilize scale augmentation like [6]. Input frames are resized with the shortest side being at least 480 and at most 800 pixels, and longest side is at most 800.

In the other datasets [8], [9], the learning rate is dropped by 10 times at every 60 epochs with a batch size of 16. We use a scale augmentation scheme similar to the one used for AG, except that the longest side of the resized image is chosen as 1333. The training schedule is selected based on the convergence of losses. Upon acceptance, we will publicly release our trained models and code.

Object Spatial Decoder	Relation Spatial Decoder	Unseen (mAP)	Seen (mAP)
3	3	20.2	31.4
3	6	20.8	31.8
6	3	21.1	31.7
6	6	18.0	31.3

TABLE VIII
DIFFERENT NUMBER OF LAYERS IN THE OBJECT SPATIAL DECODER AND THE RELATION SPATIAL DECODER.

V. RESULTS & ANALYSIS

In this section, we first compare DDS’s performance with the SOTA models in Section V-A. Next, a detailed study on the impact of different components of our network is presented in Section V-B. Finally, in Section V-C qualitative results from our model are provided.

A. Comparison with the SOTA models

In the AG [7] dataset, we report DDS’s performances in Table I under the compositional setting. In this setting, there are $\sim 12\%$ less training data with 80 unseen relationship triplets. We retrain the SOTA model STTran [5] in the mentioned setting for comparison. It is important to note here, among the three recent DSG generation models [3]–[5], only STTran’s code is publicly available, therefore limiting the capacity to evaluate other models. DDS outperforms STTran in all recall levels in both unseen and seen relationship triplet detection. Especially, for detecting unseen triplets DDS achieves 4 – 24 times improvement over the SOTA model. It shows the generalization power of DDS.

Additionally, for a fair comparison with other models, we train DDS in the full training set of AG dataset and report performance in Table II. Here, all methods up to VCTree [12] are SSG generation methods implemented by [5]. As expected, with similar training data like other models in Table II, DDS achieves SOTA performance on all metrics.

In Table III and Table IV, DDS outperforms all existing methods in HICO-Det [8] and UnRel [9] datasets. Among these methods, [65] and [55] follow a Transformer based encoder-decoder architecture. The proposed network shows superior performance than both of the models. In summary, DDS outperforms existing works in both seen and unseen SSG generation (full category) in HICO-Det by 5% and in UnRel by 33%.

B. Ablation Studies

We perform ablations for different design choices of our network in this section. For these ablations, we report our performances in the HICO-Det [8] dataset.

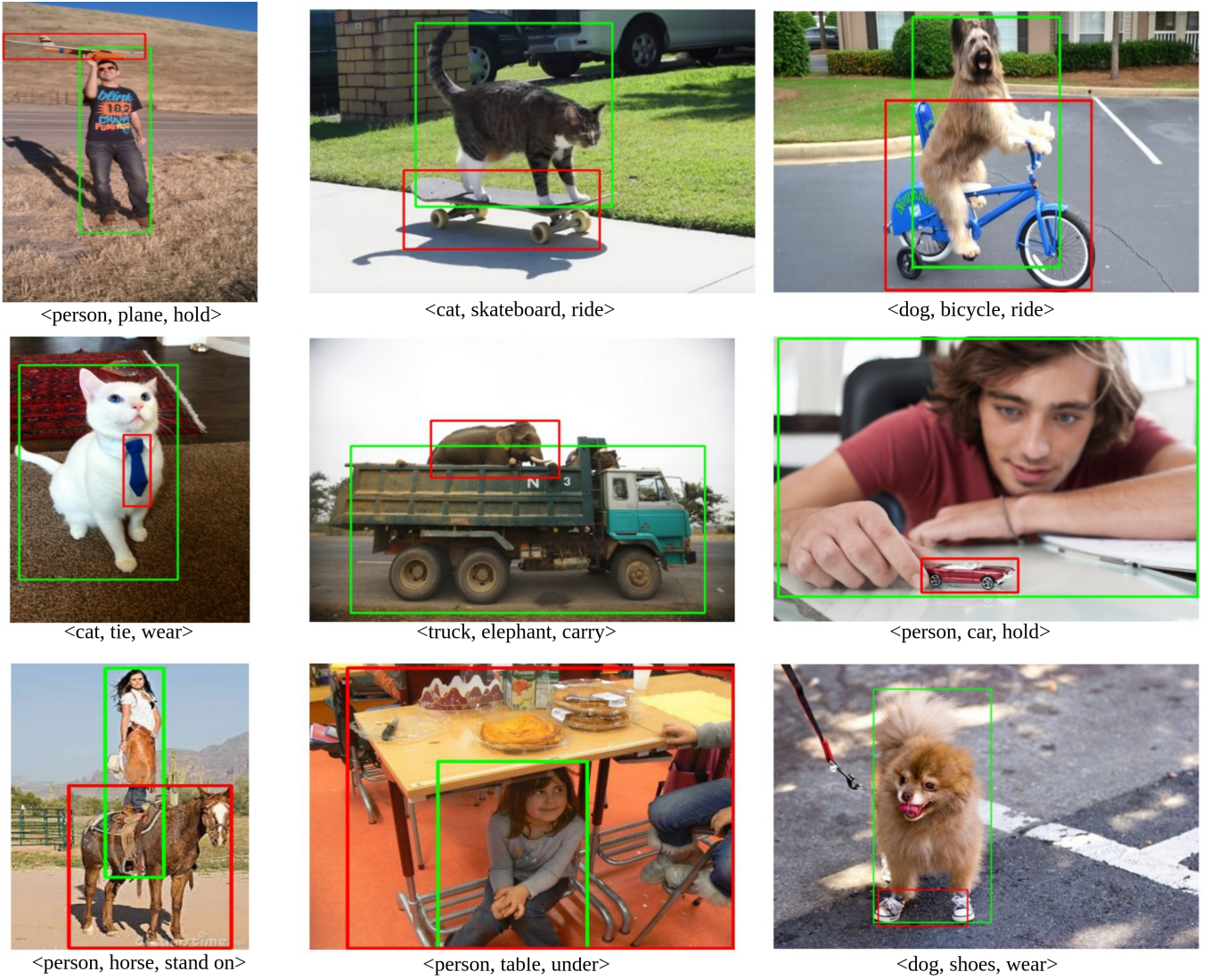


Fig. 4. Qualitative results of DDS for predicting unusual relationship triplets in UnRel [9] dataset. The subject bounding box is green and the object bounding box is red. *Our base network (single branch) fails to detect these marked triplets.* For both networks, we utilize top-20 predictions per sample.

Multi-branch Design: We first validate our decoupled multi-branch design. The performances are reported in Table V. The base network has one single branch where a single set of queries is used for both relationship and object detection. In row 1 of Table V the performance is pretty poor for the single branch base network, especially in the unseen category. Next, a multi-branch network is created by using two spatio-temporal decoders. Both decoders get the same encoded features. However, the relation branch in this case doesn't do relation region prediction. A performance improvement is observed compared to the single branch for this design. Similarly, with the gradual introduction of two encoders and relation region prediction, the performance keeps increasing. In particular, all these components yield a significant improvement in the unseen category compared to the seen category and thus show the impact of decoupled learning on unseen relationship triplet predictions. We also do qualitative analysis between DDS and the base network described in the section V-C.

Relation Region Ground Truths: As noted in Section III-F

the relation branch only produces relation region prediction during training. Ground truth relation region is required for the training. However, ground truth relation regions are not strictly defined by the provided annotations such as subject and object bounding boxes. Therefore, we experiment with different settings to generate ground truth relation regions for subject and object pairs that have relationships:

- **Mixture:** In this case, the intersection of the subject, and object bounding boxes is selected as the relation region if the boxes have an IoU greater than the θ . For any other case, the relation region is defined as their union boxes. Different values of θ are tested.
- **Union box:** Here, the union of the subject and object bounding boxes is defined as the relation region.

The performances of the network with different relation region ground truths are shown in Table VII. With union boxes, DDS performs best (last row). This may be due to the fact that the union box guarantees the inclusion of the spatial location of the relation and therefore it can be very helpful in detecting

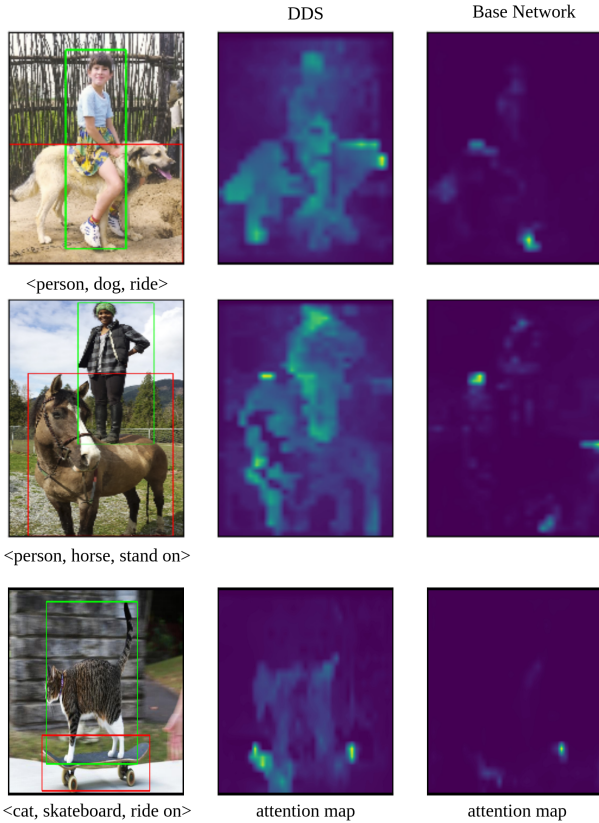


Fig. 5. Performance analysis of DDS over the base network. The subject bounding box is green and the object bounding box is red. The attention maps are visualized from the last layer of the spatio-temporal decoder.

non-contact relationship triplets (e.g. subject looks at object etc.).

Share Queries: DDS utilizes two different sets of queries for the relation and the object branches. We also test DDS’s performance by sharing the queries between the branches with two different strategies:

- DDS with o to r: In this case, the output of the object spatio-temporal decoder is fed as input relation queries to the relation spatio-temporal decoder.
- DDS with r to o: In this case, the output of the relation spatio-temporal decoder is fed as input object queries to the object spatio-temporal decoder.

The performances are reported in Table VI. Without sharing the queries DDS performs the best, especially in unseen categories. This matches our hypothesis on the importance of decoupled learning by utilizing two different sets of queries. We also notice a significant performance drop even in seen classes when we share queries from the relation to the object branch (2nd row). This shows object queries have more generalization ability than the relation queries.

Spatial Decoders: We test with different numbers of layers for spatial decoders. The result is shown in Table VIII. DDS performs poorly in extreme cases (first and last row). This is expected as DDS is getting underfitted due to the decrease in the number of layers (first row) and overfitted as the number of layers increases (last row) in the relation branch. Also, the best performance in the unseen category arises when the object

decoder has more layers than the relation decoder. Given that the object spatial decoder decodes two entities (subject, object), it is reasonable to require more layers than the relation spatial decoder.

C. Qualitative Results

This section compares DDS’s performance with our base network, a single branch network with one encoder, and one spatio-temporal decoder (details in section V-B). This comparison is made in the UnRel [9] dataset that has very unusual unseen relationship triplets. Fig. 4 illustrates the samples where DDS is successful; however, our base network completely misses the relationship triplets (predicted bounding boxes do not match with ground truth). We utilize the most confident 20 predictions for each sample from both networks for this visualization.

We compare the attention maps from DDS and the base network to further analyze our improved performances. Fig. 5 presents attention maps for the samples where both DDS and the base network have correct predictions. The attention maps are of the queries that predict the marked subject and object bounding boxes from the last layer of the spatio-temporal decoders. We overlap attention maps from both our spatio-temporal decoders to get the final attention map. As can be seen, although both networks have correct predictions, DDS’s attention maps cover the correct spatial region. In contrast, the base network with only one spatio-temporal decoder has attention on a very random portion of the object and the subject.

VI. CONCLUSION

This paper proposes a multi-branch decoupled network for DSG generation. The DDS network is comprised of two encoder-decoder based Transformer branches. This design enables independent learning of objects and relationships, thus enabling DDS to detect unseen relationship triplets. The effectiveness of DDS is demonstrated through extensive experiments with DDS achieving SOTA performance on three benchmark datasets. Moreover, the conducted ablation studies have provided the motivation and significance for different components of DDS. However, while successful compared to the existing works, the quantitative results (Table II, III, IV) show room for improvement in detecting unseen relationship triplets. Future research will focus on improving DDS for a better generalized DSG generation.

ACKNOWLEDGMENTS

This research is partially supported by the following grants: US Army Research Laboratory (ARL) under agreement number W911NF2020157; and by NSF award SI2-SSI #1664172. The U.S. Government is authorized to reproduce and distribute reprints for Governmental purposes notwithstanding any copyright notation thereon. The views and conclusions contained herein are those of the authors and should not be interpreted as necessarily representing the official policies or endorsements, either expressed or implied, of US Army Research Laboratory (ARL) or the U.S. Government.

REFERENCES

- [1] O. Ulutun, S. Rallapalli, M. Srivatsa, C. Torres, and B. Manjunath, "Actor conditioned attention maps for video action detection," in *Proceedings of the IEEE/CVF Winter Conference on Applications of Computer Vision*, 2020, pp. 527–536.
- [2] X. Liu, P. Ghosh, O. Ulutun, B. Manjunath, K. Chan, and R. Govindan, "Caesar: cross-camera complex activity recognition," in *Proceedings of the 17th Conference on Embedded Networked Sensor Systems*, 2019, pp. 232–244.
- [3] J. Ji, R. Desai, and J. C. Niebles, "Detecting human-object relationships in videos," in *Proceedings of the IEEE/CVF International Conference on Computer Vision*, 2021, pp. 8106–8116.
- [4] Y. Li, X. Yang, and C. Xu, "Dynamic scene graph generation via anticipatory pre-training," in *Proceedings of the IEEE/CVF Conference on Computer Vision and Pattern Recognition*, 2022, pp. 13 874–13 883.
- [5] Y. Cong, W. Liao, H. Ackermann, B. Rosenhahn, and M. Y. Yang, "Spatial-temporal transformer for dynamic scene graph generation," in *Proceedings of the IEEE/CVF International Conference on Computer Vision*, 2021, pp. 16 372–16 382.
- [6] N. Carion, F. Massa, G. Synnaeve, N. Usunier, A. Kirillov, and S. Zagoruyko, "End-to-end object detection with transformers," in *European conference on computer vision*. Springer, 2020, pp. 213–229.
- [7] J. Ji, R. Krishna, L. Fei-Fei, and J. C. Niebles, "Action genome: Actions as compositions of spatio-temporal scene graphs," in *Proceedings of the IEEE/CVF Conference on Computer Vision and Pattern Recognition*, 2020, pp. 10 236–10 247.
- [8] Y.-W. Chao, Y. Liu, X. Liu, H. Zeng, and J. Deng, "Learning to detect human-object interactions," in *2018 IEEE winter conference on applications of computer vision (wacv)*. IEEE, 2018, pp. 381–389.
- [9] J. Peyre, J. Sivic, I. Laptev, and C. Schmid, "Weakly-supervised learning of visual relations," in *Proceedings of the IEEE international conference on computer vision*, 2017, pp. 5179–5188.
- [10] J. Johnson, R. Krishna, M. Stark, L.-J. Li, D. Shamma, M. Bernstein, and L. Fei-Fei, "Image retrieval using scene graphs," in *Proceedings of the IEEE conference on computer vision and pattern recognition*, 2015, pp. 3668–3678.
- [11] Y. Lu, H. Rai, J. Chang, B. Knyazev, G. Yu, S. Shekhar, G. W. Taylor, and M. Volkovs, "Context-aware scene graph generation with seq2seq transformers," in *Proceedings of the IEEE/CVF International Conference on Computer Vision*, 2021, pp. 15 931–15 941.
- [12] K. Tang, H. Zhang, B. Wu, W. Luo, and W. Liu, "Learning to compose dynamic tree structures for visual contexts," in *Proceedings of the IEEE/CVF conference on computer vision and pattern recognition*, 2019, pp. 6619–6628.
- [13] Y. Cong, H. Ackermann, W. Liao, M. Y. Yang, and B. Rosenhahn, "Nodis: Neural ordinary differential scene understanding," in *European Conference on Computer Vision*. Springer, 2020, pp. 636–653.
- [14] W. Wang, R. Wang, S. Shan, and X. Chen, "Exploring context and visual pattern of relationship for scene graph generation," in *Proceedings of the IEEE/CVF Conference on Computer Vision and Pattern Recognition*, 2019, pp. 8188–8197.
- [15] J. Shi, Y. Zhong, N. Xu, Y. Li, and C. Xu, "A simple baseline for weakly-supervised scene graph generation," in *Proceedings of the IEEE/CVF International Conference on Computer Vision*, 2021, pp. 16 393–16 402.
- [16] W. Wang, R. Wang, and X. Chen, "Topic scene graph generation by attention distillation from caption," in *Proceedings of the IEEE/CVF International Conference on Computer Vision*, 2021, pp. 15 900–15 910.
- [17] L. Chen, H. Zhang, J. Xiao, X. He, S. Pu, and S.-F. Chang, "Counterfactual critic multi-agent training for scene graph generation," in *Proceedings of the IEEE/CVF International Conference on Computer Vision*, 2019, pp. 4613–4623.
- [18] M.-J. Chiou, H. Ding, H. Yan, C. Wang, R. Zimmermann, and J. Feng, "Recovering the unbiased scene graphs from the biased ones," in *Proceedings of the 29th ACM International Conference on Multimedia*, 2021, pp. 1581–1590.
- [19] H.-S. Fang, Y. Xie, D. Shao, and C. Lu, "Dirv: Dense interaction region voting for end-to-end human-object interaction detection," in *The AAAI Conference on Artificial Intelligence (AAAI)*, 2021.
- [20] C. Gao, Y. Zou, and J.-B. Huang, "ican: Instance-centric attention network for human-object interaction detection," in *British Machine Vision Conference*, 2018.
- [21] Y.-L. Li, S. Zhou, X. Huang, L. Xu, Z. Ma, H.-S. Fang, Y. Wang, and C. Lu, "Transferable interactiveness knowledge for human-object interaction detection," in *Proceedings of the IEEE Conference on Computer Vision and Pattern Recognition*, 2019, pp. 3585–3594.
- [22] Y. Liu, Q. Chen, and A. Zisserman, "Amplifying key cues for human-object-interaction detection," in *European Conference on Computer Vision*. Springer, 2020, pp. 248–265.
- [23] B. Wan, D. Zhou, Y. Liu, R. Li, and X. He, "Pose-aware multi-level feature network for human object interaction detection," in *Proceedings of the IEEE International Conference on Computer Vision*, 2019, pp. 9469–9478.
- [24] T. Wang, R. M. Anwer, M. H. Khan, F. S. Khan, Y. Pang, L. Shao, and J. Laaksonen, "Deep contextual attention for human-object interaction detection," in *Proceedings of the IEEE International Conference on Computer Vision*, 2019, pp. 5694–5702.
- [25] C. Gao, J. Xu, Y. Zou, and J.-B. Huang, "Drg: Dual relation graph for human-object interaction detection," in *Proc. European Conference on Computer Vision (ECCV)*, 2020.
- [26] O. Ulutun, A. Iftekhar, and B. S. Manjunath, "Vsgnet: Spatial attention network for detecting human object interactions using graph convolutions," in *Proceedings of the IEEE/CVF Conference on Computer Vision and Pattern Recognition*, 2020, pp. 13 617–13 626.
- [27] X. Zhong, C. Ding, X. Qu, and D. Tao, "Polysemy deciphering network for human-object interaction detection," in *Proc. Eur. Conf. Comput. Vis*, 2020.
- [28] D.-J. Kim, X. Sun, J. Choi, S. Lin, and I. S. Kweon, "Detecting human-object interactions with action co-occurrence priors," in *European Conference on Computer Vision*. Springer, 2020, pp. 718–736.
- [29] Y. Liu, J. Yuan, and C. W. Chen, "Consnet: Learning consistency graph for zero-shot human-object interaction detection," in *Proceedings of the 28th ACM International Conference on Multimedia*, 2020, pp. 4235–4243.
- [30] Z. Hou, X. Peng, Y. Qiao, and D. Tao, "Visual compositional learning for human-object interaction detection," in *ECCV*, 2020.
- [31] H. Wang, W.-s. Zheng, and L. Yingbiao, "Contextual heterogeneous graph network for human-object interaction detection," in *European Conference on Computer Vision*. Springer, 2020, pp. 248–264.
- [32] Y.-L. Li, X. Liu, X. Wu, Y. Li, and C. Lu, "Hoi analysis: Integrating and decomposing human-object interaction," in *Advances in Neural Information Processing Systems*, H. Larochelle, M. Ranzato, R. Hadsell, M. F. Balcan, and H. Lin, Eds., vol. 33. Curran Associates, Inc., 2020, pp. 5011–5022.
- [33] D. Xu, Y. Zhu, C. B. Choy, and L. Fei-Fei, "Scene graph generation by iterative message passing," in *Proceedings of the IEEE conference on computer vision and pattern recognition*, 2017, pp. 5410–5419.
- [34] R. Zellers, M. Yatskar, S. Thomson, and Y. Choi, "Neural motifs: Scene graph parsing with global context," in *Proceedings of the IEEE conference on computer vision and pattern recognition*, 2018, pp. 5831–5840.
- [35] A. Iftekhar, S. Kumar, R. A. McEver, S. You, and B. Manjunath, "Gtnet: Guided transformer network for detecting human-object interactions," *arXiv preprint arXiv:2108.00596*, 2021.
- [36] A. Iftekhar, H. Chen, K. Kundu, X. Li, J. Tighe, and D. Modolo, "What to look at and where: Semantic and spatial refined transformer for detecting human-object interactions," in *Proceedings of the IEEE/CVF Conference on Computer Vision and Pattern Recognition*, 2022, pp. 5353–5363.
- [37] B. Kim, J. Lee, J. Kang, E.-S. Kim, and H. J. Kim, "Hotr: End-to-end human-object interaction detection with transformers," in *Proceedings of the IEEE/CVF Conference on Computer Vision and Pattern Recognition*, 2021, pp. 74–83.
- [38] M. Tamura, H. Ohashi, and T. Yoshinaga, "Qpic: Query-based pairwise human-object interaction detection with image-wide contextual information," in *Proceedings of the IEEE/CVF Conference on Computer Vision and Pattern Recognition*, 2021, pp. 10 410–10 419.
- [39] M. Chen, Y. Liao, S. Liu, Z. Chen, F. Wang, and C. Qian, "Reformulating hoi detection as adaptive set prediction," in *Proceedings of the IEEE/CVF Conference on Computer Vision and Pattern Recognition*, 2021, pp. 9004–9013.
- [40] C. Zou, B. Wang, Y. Hu, J. Liu, Q. Wu, Y. Zhao, B. Li, C. Zhang, C. Zhang, Y. Wei *et al.*, "End-to-end human object interaction detection with hoi transformer," in *Proceedings of the IEEE/CVF Conference on Computer Vision and Pattern Recognition*, 2021, pp. 11 825–11 834.
- [41] B. Kim, J. Mun, K.-W. On, M. Shin, J. Lee, and E.-S. Kim, "Mstr: Multi-scale transformer for end-to-end human-object interaction detection," in *Proceedings of the IEEE/CVF Conference on Computer Vision and Pattern Recognition*, 2022, pp. 19 578–19 587.
- [42] A. Zhang, Y. Liao, S. Liu, M. Lu, Y. Wang, C. Gao, and X. Li, "Mining the benefits of two-stage and one-stage hoi detection," *Advances in Neural Information Processing Systems*, vol. 34, pp. 17 209–17 220, 2021.

- [43] Y. Liao, A. Zhang, M. Lu, Y. Wang, X. Li, and S. Liu, "Gen-vlkt: Simplify association and enhance interaction understanding for hoi detection," in *Proceedings of the IEEE/CVF Conference on Computer Vision and Pattern Recognition*, 2022, pp. 20 123–20 132.
- [44] J. Park, S. Lee, H. Heo, H. K. Choi, and H. J. Kim, "Consistency learning via decoding path augmentation for transformers in human object interaction detection," in *Proceedings of the IEEE/CVF Conference on Computer Vision and Pattern Recognition*, 2022, pp. 1019–1028.
- [45] D. Zhou, Z. Liu, J. Wang, L. Wang, T. Hu, E. Ding, and J. Wang, "Human-object interaction detection via disentangled transformer," in *Proceedings of the IEEE/CVF Conference on Computer Vision and Pattern Recognition*, 2022, pp. 19 568–19 577.
- [46] X. Qu, C. Ding, X. Li, X. Zhong, and D. Tao, "Distillation using oracle queries for transformer-based human-object interaction detection," in *Proceedings of the IEEE/CVF Conference on Computer Vision and Pattern Recognition*, 2022, pp. 19 558–19 567.
- [47] A. Radford, J. W. Kim, C. Hallacy, A. Ramesh, G. Goh, S. Agarwal, G. Sastry, A. Askell, P. Mishkin, J. Clark *et al.*, "Learning transferable visual models from natural language supervision," in *International Conference on Machine Learning*. PMLR, 2021, pp. 8748–8763.
- [48] I. Misra, A. Gupta, and M. Hebert, "From red wine to red tomato: Composition with context," in *Proceedings of the IEEE Conference on Computer Vision and Pattern Recognition*, 2017, pp. 1792–1801.
- [49] K. Wei, M. Yang, H. Wang, C. Deng, and X. Liu, "Adversarial fine-grained composition learning for unseen attribute-object recognition," in *Proceedings of the IEEE/CVF International Conference on Computer Vision (ICCV)*, October 2019.
- [50] S. Purushwalkam, M. Nickel, A. Gupta, and M. Ranzato, "Task-driven modular networks for zero-shot compositional learning," in *Proceedings of the IEEE/CVF International Conference on Computer Vision*, 2019, pp. 3593–3602.
- [51] M. F. Naeem, Y. Xian, F. Tombari, and Z. Akata, "Learning graph embeddings for compositional zero-shot learning," in *Proceedings of the IEEE/CVF Conference on Computer Vision and Pattern Recognition*, 2021, pp. 953–962.
- [52] S. Kumar, A. Iftekhhar, E. Prashnani, and B. Manjunath, "Locl: Learning object-attribute composition using localization," *arXiv preprint arXiv:2210.03780*, 2022.
- [53] K. Kato, Y. Li, and A. Gupta, "Compositional learning for human object interaction," in *Proceedings of the European Conference on Computer Vision (ECCV)*, 2018, pp. 234–251.
- [54] Z. Hou, B. Yu, Y. Qiao, X. Peng, and D. Tao, "Affordance transfer learning for human-object interaction detection," in *CVPR*, 2021.
- [55] Z. Hou, B. Yu, and D. Tao, "Discovering human-object interaction concepts via self-compositional learning," in *ECCV*, 2022.
- [56] Z. Hou, B. Yu, Y. Qiao, X. Peng, and D. Tao, "Detecting human-object interaction via fabricated compositional learning," in *Proceedings of the IEEE/CVF Conference on Computer Vision and Pattern Recognition*, 2021, pp. 14 646–14 655.
- [57] K. He, X. Zhang, S. Ren, and J. Sun, "Deep residual learning for image recognition," in *Proceedings of the IEEE conference on computer vision and pattern recognition*, 2016, pp. 770–778.
- [58] A. Vaswani, N. Shazeer, N. Parmar, J. Uszkoreit, L. Jones, A. N. Gomez, L. Kaiser, and I. Polosukhin, "Attention is all you need," *Advances in neural information processing systems*, vol. 30, 2017.
- [59] S. Qi, W. Wang, B. Jia, J. Shen, and S.-C. Zhu, "Learning human-object interactions by graph parsing neural networks," in *Proceedings of the European conference on computer vision (ECCV)*, 2018, pp. 401–417.
- [60] Y. Liao, S. Liu, F. Wang, Y. Chen, C. Qian, and J. Feng, "Ppdm: Parallel point detection and matching for real-time human-object interaction detection," in *Proceedings of the IEEE/CVF Conference on Computer Vision and Pattern Recognition*, 2020, pp. 482–490.
- [61] C. Lu, R. Krishna, M. Bernstein, and L. Fei-Fei, "Visual relationship detection with language priors," in *European conference on computer vision*. Springer, 2016, pp. 852–869.
- [62] Y. Li, W. Ouyang, B. Zhou, K. Wang, and X. Wang, "Scene graph generation from objects, phrases and region captions," in *Proceedings of the IEEE international conference on computer vision*, 2017, pp. 1261–1270.
- [63] J. Yang, J. Lu, S. Lee, D. Batra, and D. Parikh, "Graph r-cnn for scene graph generation," in *Proceedings of the European conference on computer vision (ECCV)*, 2018, pp. 670–685.
- [64] K. Tang, Y. Niu, J. Huang, J. Shi, and H. Zhang, "Unbiased scene graph generation from biased training," in *Proceedings of the IEEE/CVF conference on computer vision and pattern recognition*, 2020, pp. 3716–3725.
- [65] S. Wang, Y. Duan, H. Ding, Y.-P. Tan, K.-H. Yap, and J. Yuan, "Learning transferable human-object interaction detector with natural language supervision," in *Proceedings of the IEEE/CVF Conference on Computer Vision and Pattern Recognition*, 2022, pp. 939–948.
- [66] J. Peyre, I. Laptev, C. Schmid, and J. Sivic, "Detecting unseen visual relations using analogies," in *Proceedings of the IEEE/CVF International Conference on Computer Vision*, 2019, pp. 1981–1990.
- [67] G. A. Sigurdsson, G. Varol, X. Wang, A. Farhadi, I. Laptev, and A. Gupta, "Hollywood in homes: Crowdsourcing data collection for activity understanding," in *European Conference on Computer Vision*. Springer, 2016, pp. 510–526.
- [68] L. Ilya, H. Frank *et al.*, "Decoupled weight decay regularization," *Proceedings of ICLR*, 2019.
- [69] T.-Y. Lin, M. Maire, S. Belongie, J. Hays, P. Perona, D. Ramanan, P. Dollár, and C. L. Zitnick, "Microsoft coco: Common objects in context," in *European conference on computer vision*. Springer, 2014, pp. 740–755.